Available online at www.sciencedirect.com
SCIENCE DIRECT®
International Journal of Solids and Structures 41 (2004) 6441–6463
INTERNATIONAL JOURNAL OF SOLIDS and STRUCTURES
www.elsevier.com/locate/ijsolstr

Post-severance analysis of impulsively loaded beams

Norman Jones [a,*], Marcílio Alves [b,*]

[a] Impact Research Centre, Department of Engineering (Mechanical), University of Liverpool, Liverpool, L69 3GH UK
[b] Department of Mechatronics and Mechanical Systems Engineering, University of São Paulo, São Paulo, 05508-900, Brazil

Received 28 August 2003; accepted 29 April 2004
Available online 17 June 2004

Abstract

The dynamic energy imparted to structures can cause material failure. The present investigation considers such a failure for a simply supported beam which is subjected to a blast loading idealised as an initial velocity distributed uniformly throughout the span. The theoretical solutions are developed using a rigid, perfectly plastic idealization and are exact within the context of dynamic plasticity. A simple failure criterion, shown to be derived from Continuum Damage Mechanics, is used in the calculations. Attention is focused on the motion of the beam after it fails and becomes detached from supports. It is shown that a considerable amount of energy remains in the beam after failure, which depends on the beam geometry. Part of this energy is consumed in changing the beam shape after severance, with the remainder as kinetic energy of the beam travelling as a rigid body.

Keywords: Beam; Impulsive loading; Rigid-plastic material; Failure; Post-failure response; Continuum Damage Mechanics

1. Introduction

The inelastic response of structures under large impact loads has found important applications in the design of energy absorbing and collision protection devices for transportation systems (Johnson, 1990). In particular, the dynamic behaviour of free–free beams can be relevant in the aerospace industry. It was found, for example, that a rigid, perfectly plastic free–free beam subjected to a triangular shaped pressure pulse absorbs only 1/4 of the input energy, with the remaining 3/4 manifested as a rigid body motion (Jones and Wierzbicki, 1987).

Yu et al. (2001) examined the problem of a free–free beam which collides with a cantilever beam. The authors used an analytical–numerical approach to predict the partitioning of energy between the two structures. They also obtained an approximate transverse shear failure map by assuming that failure occurred when any shear sliding equalled the beam thickness. The dynamic behaviour of free–free beams was also studied by Yu et al. (1996). The authors used a numerical approach to investigate elastic effects on

* Corresponding authors. Tel.: +55-11-30915757/+44-151-7944848; fax: +44-151-7944858.
E-mail addresses: norman.jones@liv.ac.uk (N. Jones), maralves@usp.br (M. Alves).

0020-7683/$ - see front matter © 2004 Elsevier Ltd. All rights reserved.
doi:10.1016/j.ijsolstr.2004.04.042

Nomenclature

D	damage parameter
E	elastic modulus
H	beam thickness
k	material constant
K	kinetic energy
K_{i}	initial kinetic energy
K_{r}	residual kinetic energy
$K_{\mathrm{b_m}}$	bending energy absorbed by the moving hinge
$k_{\mathrm{b_r}}$	bending energy absorbed at mid-span (Fig. 4)
$K_{\mathrm{b_s}}$	bending energy absorbed by the stationary hinge
$K_{\mathrm{s_s}}$	shear energy absorbed at the support
$2L$	beam length
m	beam mass per unit length
M	bending moment
M_0	bending moment for plastic collapse
Q	transverse shear force
Q_0	transverse shear force for plastic collapse
r_1 and r_2	energy ratios
$R_{\bar{v}}$	defined by Eq. (101)
$\bar{S}$	material constant
t_{h_0}	time when the moving hinges reach the beam centre
t_{f}	final time
t	time
t_{fa}	time to failure
t_3	duration of final phase of motion
t_{r}	time when a rigid body motion is initiated
V_0	impulsive velocity
$V_{0_{\mathrm{c}}}$	threshold impulsive (critical) velocity
$\bar{V}_{0_{\mathrm{c}}}$	dimensionless critical velocity
$\bar{x}$	dimensionless coordinate
W	displacement
W_3	beam displacement in the final phase of motion
$W_{\bar{0}}$	mid-span transverse displacement at failure
W_{f}	final beam displacement
W_{f_1}	beam displacement at the support after the transient phase
W_{f_2}	beam displacement at the mid-span after the transient phase
W_{s}	transverse shear displacement at the beam support
$W_{\bar{\mathrm{s}}}$	transverse shear displacement at the beam support at failure
$\dot{W}_{\mathrm{s}}$	transverse shear velocity at the beam support
$\dot{W}_{1_{\mathrm{r}}}$	rigid body velocity of the beam
$(\cdot)$	time derivative of ( )
$(\cdot\cdot)$	second time derivative of ( )
α	defined by Eq. (10)
β	defined by Eq. (36)

ε_D	threshold damage strain
v	defined by Eq. (1)
σ_0	flow stress
$\bar{\xi}$	dimensionless plastic hinge position
$\bar{\xi}_0$	dimensionless initial plastic hinge position

the response of free–free beams subjected to impact by a projectile at the mid-span or to triangular distributed impulsive loadings.

Yang et al. (1998) studied the response of rigid, perfectly plastic beams subjected to a step-load at various positions along the beam span. This theoretical study was further explored by Yang and Xi (2003) for a concentrated impact load at any position along the beam span, and comparisons were made with experimental data and a numerical model.

A common approach for the analysis of structures impacted with large loads assumes that the material is rigid-perfectly plastic, i.e. a material with no elastic deformation and a constant flow stress, regardless of the strain level. Numerical schemes are used to perform the complex analysis of real structures under impact loading (Bammann et al., 1993; Holmes et al., 1993). However, the details yielded by these analyses are in some cases less important from an engineering perspective than some global parameters, for example, maximum permanent displacement and the associated impact energy absorbed, at least during the preliminary design phase of a component. Such features of a problem can also be obtained from the rigid-plastic methods of analysis.

One interesting aspect of the dynamic analysis of a structure is that, whereas in the static case, transverse shear effects are potentially important only for short beams, this is not so when a beam is loaded dynamically (Jones and Oliveira, 1979). Transverse shear can dominate the dynamic response even for long beams, causing material failure due to shear (Jouri and Jones, 1988; Alves and Jones, 2002b).

The behaviour of a simply supported rigid, perfectly plastic beam subjected to an impulsive load may present several patterns of motion, depending on the material and geometrical characteristics. For instance, shearing deformations can develop and remain at the supports throughout motion, while in other cases, it is followed by bending at the mid-span. Shearing can also develop in an initial phase at the supports and then followed by a phase which is dominated by propagating plastic hinges moving towards the mid-span. The kinetic energy remaining in the beam is absorbed in a final phase of motion with bending at the mid-span. These features of a dynamic beam response have been studied previously by many authors (Jones, 1989).

It appears that little attention has been paid to the motion of a beam after failure which is of interest in forensic analysis, for example. A beam, upon failure, might still possess a residual kinetic energy. Part of this kinetic energy is dissipated internally and causes a post-failure shape change of the beam, while, to conserve momentum, part remains in the beam to propel it as a rigid body.

This article aims to extend the analysis detailed by Jones (1989) for the case of a simply supported beam under a blast load by studying the behaviour of the beam after material failure due to excessive shear strains. A failure criterion is necessary in order to estimate the conditions for the beam to break free from its support. The failure criterion here used is shown to be derived from Continuum Damage Mechanics.

The beam depicted in Fig. 1 has a length $2L$ and a doubly symmetric cross-section. The beam is loaded with an initial impulsive velocity V_0, which is distributed uniformly across the entire span, and is made from a rigid, perfectly, plastic material with a flow stress σ_0.

It is convenient to introduce the parameter

$$v = LQ_0/2M_0, \tag{1}$$

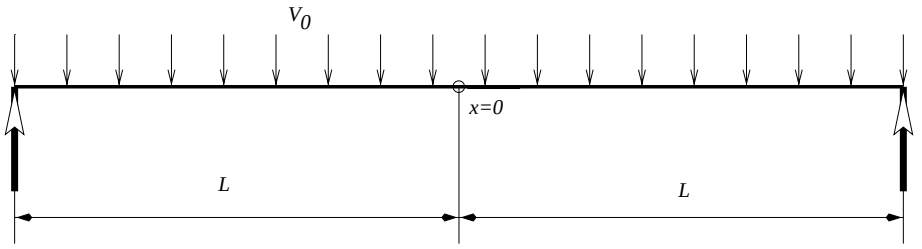

Fig. 1. A simply supported beam under an impulsive load.

which is a dimensionless ratio between the transverse shear collapse force, Q_0, and the bending moment, M_0, acting on a beam cross-section.

It is shown in Jones (1989) that various theoretical solutions for simply supported beams loaded impulsively are related to the value of v. Here, these solutions, which are valid for small deformations and rotations, are expanded for the case when failure occurs at the supports. The use of a small deformation theory is justified since finite-deflection (i.e., membrane) effects are not significant during the initial shearing phase when the displacements remain small. They are also not significant after severance since no membrane forces will develop because there is no axial restraint.

2. Beams with $v \leqslant 1$

For this class of beams, it is shown in Jones (1989) that only transverse shear sliding occurs at the supports, Fig. 2. Hence, the whole beam remains straight and moves down as a rigid body. Eventually, for a sufficiently large input energy, complete severance occurs at the supports and the detached beam travels throughout space with a finite velocity.

The threshold condition for severance can be determined only upon the application of a failure criterion. Jones (1976) has suggested that complete severance occurs when

$$W_s \geqslant kH, \tag{2}$$

where $0 \leqslant k \leqslant 1$ is a material constant and H is the beam depth.

The transverse shear displacement for this beam according to Jones (1989) is

$$W_s = -Q_0 t^2/2mL + V_0 t, \tag{3}$$

where m is the beam mass per unit length and t is time. Substituting Eq. (3) into the equality of Eq. (2) gives

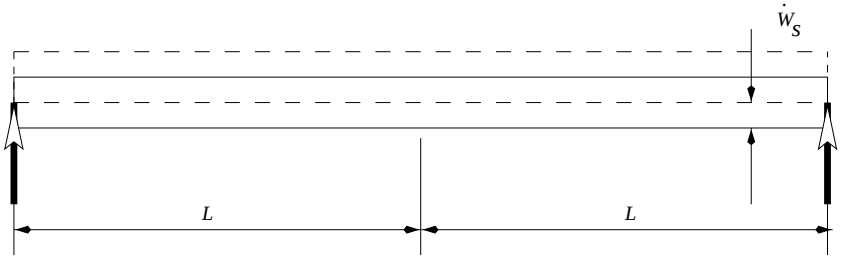

Fig. 2. Transverse shear slides at the supports of a simply supported beam with $v \leqslant 1$ loaded impulsively.

$$t_{\mathrm{fa}} = \frac{mLV_0}{Q_0}\left[1 - \sqrt{1 - \frac{2kHQ_0}{mLV_0^2}}\right], \tag{4}$$

which is the time when the beam is severed. Hence, the beam travels after complete severance with a velocity

$$\dot{W}_{\bar{\mathrm{s}}} = V_0\sqrt{1 - \frac{2kHQ_0}{mLV_0^2}}. \tag{5}$$

It should be noted that Eq. (5) gives a threshold value for the initial impulsive velocity which causes severance, i.e.

$$V_{0_{\mathrm{c}}} = \sqrt{\frac{2kHQ_0}{mL}} = \sqrt{\frac{4kHvM_0}{mL^2}} \tag{6}$$

at $\dot{W}_{\bar{\mathrm{s}}} = 0$.

Thus, for such a class of short beams, the beam with $Q = 0$ at $x = \pm L$ would travel freely with the velocity given by Eq. (5) for initial impulsive velocities $V_0 > V_{0_{\mathrm{c}}}$ and with the straight profile depicted in Fig. 2.

It is proved in Appendix A that the changed boundary conditions are consistent with a straight profile and that no further plastic deformation takes place, i.e. the solution is statically and kinematically admissible and, therefore, exact.

3. Beams with $1 \leqslant v \leqslant 3/2$

For this category of beams, the boundary conditions change once severance occurs due to a transverse shear failure at the supports during, or in the limiting case, at the end of the first phase of motion.

A possible velocity profile necessary to establish a theoretical kinematically admissible solution at severance is shown in Fig. 3. The velocities at $x = 0$ and $x = L$ are different which, after some time, become equal and allow a rigid body motion to be reached.

3.1. Motion before severance

The velocity $\dot{W}_{\mathrm{s}}$ at the supports and $\dot{W}$ at the centre are given in Reference (Jones, 1989) and can be integrated to yield the displacements at $\bar{x} = 1$ and at $\bar{x} = 0$,

$$W_{\mathrm{s}} = M_0(3 - 4v)t^2/mL^2 + V_0 t \tag{7}$$

and

$$W_0 = M_0(2v - 3)t^2/mL^2 + V_0 t, \tag{8}$$

respectively, where $\bar{x} = x/L \in [0, 1]$ is a dimensionless coordinate.

Now, $W_{\mathrm{s}} = W_{\bar{\mathrm{s}}} = kH$ in Eq. (7) when using the failure criterion in Eq. (2), so that the beam fails at the support when

$$t_{\mathrm{fa}} = L\alpha/\{2(4v - 3)M_0\}, \tag{9}$$

where

$$\alpha = mLV_0 - \sqrt{(mLV_0)^2 - 4mkHM_0(4v - 3)}. \tag{10}$$

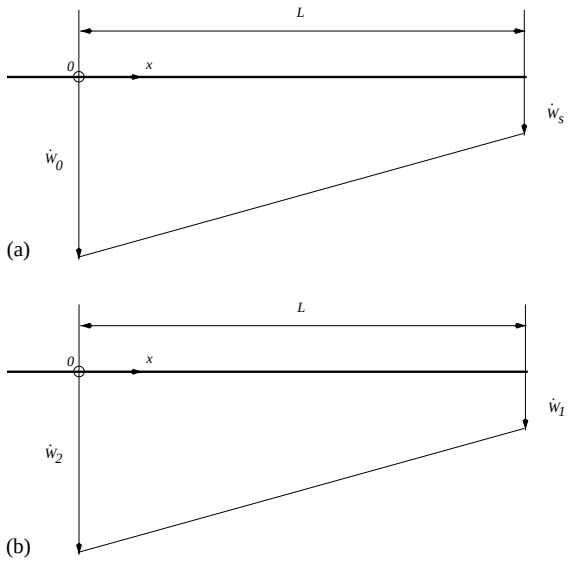

Fig. 3. Transverse velocity profile of one-half of a simply supported beam loaded impulsively with $1 \leqslant v \leqslant 3/2$: (a) at severance and (b) severed beam.

At this instant, the positive velocities of the beam at the support, $\dot{W}_{\bar{s}}$, and at the centre, $\dot{W}_{\bar{0}}$, are given by

$$\dot{W}_{\bar{s}} = V_0 - \alpha/mL \tag{11}$$

and

$$\dot{W}_{\bar{0}} = V_0 - (3-2v)\alpha/(4v-3)mL, \tag{12}$$

while the respective displacements are

$$W_{\bar{s}} = kH \tag{13}$$

and

$$W_{\bar{0}} = \frac{\alpha L}{2M_0(4v-3)}\left\{V_0 - \frac{(3-2v)\alpha}{2mL(4v-3)}\right\}. \tag{14}$$

From Eq. (11) one obtains the threshold velocity which causes material failure

$$V_{0_c} = \sqrt{\frac{4(4v-3)kHM_0}{mL^2}}, \tag{15}$$

when using Eq. (10) with $V_0 = V_{0_c}$.

3.2. Motion after severance

At severance, which is illustrated in Fig. 3(a), the initial conditions are shown in Fig. 3(b), which occur at a time t_{fa} given by Eq. (9), reset as $t = 0$ for the remaining analysis.

During the subsequent motion shown in Fig. 3(b), the transverse velocity at any point of the beam is

$$\dot{w} = \dot{W}_1 + (\dot{W}_2 - \dot{W}_1)(1 - \bar{x}), \tag{16}$$

where only one-half of the beam is analysed owing to symmetry about the mid-span.

The equilibrium equations relating the bending moment, M, and the transverse shear force, Q, of an unloaded beam are

$$\partial Q/\partial \bar{x} = mL\ddot{w} \quad \text{and} \quad Q = (1/L)\partial M/\partial \bar{x} \tag{17}$$

for small displacements and when neglecting rotatory inertia.

Using the velocity profile from Eq. (16), it follows that

$$\mathrm{d}^2M/\mathrm{d}\bar{x}^2 = mL^2[\ddot{W}_1 + (\ddot{W}_2 - \ddot{W}_1)(1-\bar{x})], \tag{18}$$

which can be integrated to give

$$Q = mL[\ddot{W}_1\bar{x} + (\ddot{W}_2 - \ddot{W}_1)(\bar{x} - \bar{x}^2/2)], \tag{19}$$

since $Q = 0$ at $t = 0$ and $\bar{x} = 0$.

Further integration yields

$$M = mL^2[\ddot{W}_1\bar{x}^2/2 + (\ddot{W}_2 - \ddot{W}_1)(\bar{x}^2/2 - \bar{x}^3/6)] + M_0, \tag{20}$$

when noting that $M = M_0$ at the central plastic hinge.

Now, Eqs. (19) and (20) with $Q = M = 0$ at $\bar{x} = 1$ give a system of equations for $\ddot{W}_1$ and $\ddot{W}_2$, whose solution is

$$\ddot{W}_1 = 6M_0/mL^2 \tag{21}$$

and

$$\ddot{W}_2 = -6M_0/mL^2. \tag{22}$$

Integrating Eq. (21) gives

$$\dot{W}_1 = 6M_0t/mL^2 + \dot{W}_{\mathrm{s}}, \tag{23}$$

since at $t = 0$, $\dot{W}_1 = \dot{W}_{\mathrm{s}}$, while a further integration yields the displacement

$$W_1 = 3M_0t^2/mL^2 + \dot{W}_{\mathrm{s}}t + kH, \tag{24}$$

when using $W_1 = W_{\mathrm{s}} = kH$ at $t = 0$.

The same procedure can be used to obtain the velocity and displacement of the beam at the centre ($\bar{x} = 0$), yielding

$$\dot{W}_2 = -6M_0t/mL^2 + \dot{W}_0 \tag{25}$$

and

$$W_2 = -6M_0t^2/2mL^2 + \dot{W}_0t + W_0, \tag{26}$$

where $\dot{W}_0$ and W_0 are the velocity and the displacement at the centre of the beam at severance ($t = 0$) given by Eqs. (12) and (14), respectively.

3.3. Rigid body motion

After failure, the beam travels freely in space and the velocity at the mid-span decreases with time, Eq. (25), while it increases at the support, Eq. (23). Hence, when these two velocities are equal at the time [1]

[1] The actual time is obtained by adding Eqs. (9) and (27).

$$t_{\mathrm{r}} = \frac{\alpha L}{2M_0}\,\frac{v-1}{4v-3}, \tag{27}$$

the beam travels as a rigid body, with no further plastic deformation.

The rigid body velocity of the beam is given by Eq. (23) for $t = t_{\mathrm{r}}$, with $\dot{W}_{\mathrm{s}}$ given by Eq. (11),

$$\dot{W}_{1_{\mathrm{r}}} = V_0 - \frac{v\alpha}{(4v-3)mL}. \tag{28}$$

For $v = 1$ and $v = 3/2$, Eq. (28) becomes

$$\dot{W}_{1_{\mathrm{r}}} = \sqrt{V_0^2 - 4kHM_0/mL^2} \tag{29}$$

and

$$\dot{W}_{1_{\mathrm{r}}} = V_0/2 + \sqrt{(V_0/2)^2 - 3kHM_0/mL^2}, \tag{30}$$

respectively.

It is demonstrated in Appendix A that the transverse velocity profile in Fig. 3 leads to an exact solution for the problem posed.

4. Beams with $v > 3/2$

Consider now a beam with $v > 3/2$ and the possible transverse velocity profile before severance in Fig. 4(a) given by

$$\dot{w} = V_0 \quad \text{for } 0 \leqslant \bar{x} \leqslant \bar{\xi}_0 \tag{31}$$

and

$$\dot{w} = \dot{W}_{\mathrm{s}} + (V_0 - \dot{W}_{\mathrm{s}})(1-\bar{x})/(1-\bar{\xi}_0) \quad \text{for } \bar{\xi}_0 \leqslant \bar{x} \leqslant 1. \tag{32}$$

4.1. Motion before severance

The velocity and displacement of the beam at the support before severance are given by (Jones, 1989)

$$\dot{W}_{\mathrm{s}} = -8v^2M_0t/3mL^2 + V_0 \tag{33}$$

and

$$W_{\mathrm{s}} = -4v^2M_0t^2/3mL^2 + V_0t, \tag{34}$$

respectively.

Eq. (34), with the failure criterion in Eq. (2), gives the failure time

$$t_{\mathrm{fa}} = \beta/2vM_0, \tag{35}$$

where

$$\beta = 3mL^2\left\{V_0 - \sqrt{V_0^2 - 16kHv^2M_0/3mL^2}\right\}\Big/4v. \tag{36}$$

At this instant, the portion $0 \leqslant \bar{x} \leqslant \bar{\xi}_0$ of the beam has a velocity V_0, while, for the span $\bar{\xi}_0 \leqslant \bar{x} \leqslant 1$,

$$\dot{w} = \dot{W}_{\bar{\mathrm{s}}} + (V_0 - \dot{W}_{\bar{\mathrm{s}}})(1-\bar{x})/(1-\bar{\xi}_0), \tag{37}$$

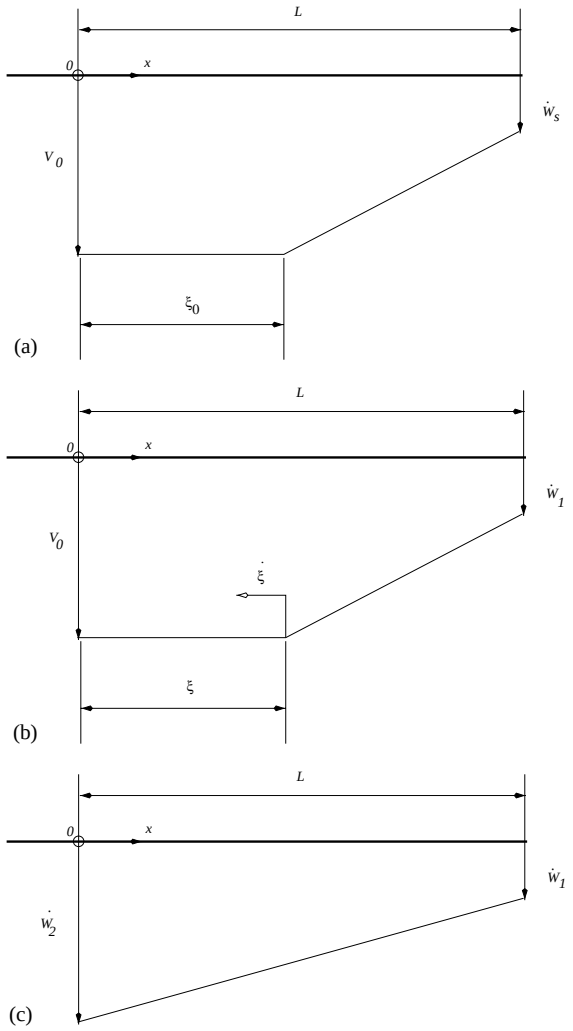

Fig. 4. Transverse velocity profiles after severance of one-half of a simply supported beam loaded impulsively with $v > 3/2$: (a) first phase of motion, (b) second phase of motion and (c) third phase of motion.

where

$$\dot{W}_s = V_0 - 4v\beta/3mL^2, \tag{38}$$

with $\bar{\xi}_0$ being the dimensionless hinge position during the first phase of motion given by

$$\bar{\xi}_0 = 1 - 3/2v. \tag{39}$$

The displacement at a support is kH and, for the central part of the beam, $0 \leqslant \bar{x} \leqslant \bar{\xi}_0$, is

$$W_2 = V_0 t_{fa} = \beta V_0/2vM_0. \tag{40}$$

Again, it is possible to obtain the critical or threshold severance velocity by setting $\dot{W}_s = 0$ in Eq. (33) and substituting the respective time into Eq. (34) when $W_s = kH$, resulting in

$$V_{0_c} = \sqrt{\frac{16kHv^2M_0}{3mL^2}}. \tag{41}$$

4.2. Motion after severance

In the next phase of motion, Fig. 4(b), the plastic hinge starts to move towards the centre of the beam so that

$$\dot{w} = \dot{W}_1 + (V_0 - \dot{W}_1)(1-\bar{x})/(1-\bar{\xi}) \quad \text{for } \bar{\xi} \leqslant \bar{x} \leqslant 1, \tag{42}$$

where $\bar{\xi} = \xi/L$ defines the dimensionless moving plastic hinge position. In order to integrate Eq. (42) to obtain the beam displacement profile, it is necessary to evaluate $\dot{W}_1$ and the time-dependence of the hinge position.

Consider then the equilibrium equation for the portion $\bar{\xi} \leqslant \bar{x} \leqslant 1$ of the beam after severance

$$\frac{d^2M}{d\bar{x}^2} = mL^2\ddot{W}_1\frac{(\bar{x}-\bar{\xi})}{(1-\bar{\xi})} + mL^2(V_0 - \dot{W}_1)\dot{\bar{\xi}}\frac{(1-\bar{x})}{(1-\bar{\xi})^2}, \tag{43}$$

which can be integrated to yield the transverse shear force

$$Q = mL\ddot{W}_1\frac{(\bar{x}^2/2 - \bar{\xi}\bar{x} + \bar{\xi}^2/2)}{(1-\bar{\xi})} + mL(V_0 - \dot{W}_1)\dot{\bar{\xi}}\frac{(\bar{x} - \bar{x}^2/2 - \bar{\xi} + \bar{\xi}^2/2)}{(1-\bar{\xi})^2}, \tag{44}$$

since $Q = 0$ at $\bar{x} = \bar{\xi}$. Integrating the above equation with the boundary condition $M = M_0$ at $\bar{x} = \bar{\xi}$, gives the bending moment distribution

$$M = M_0 + mL^2\ddot{W}_1\frac{\bar{x}^3/6 - \bar{\xi}\bar{x}^2/2 + \bar{\xi}^2\bar{x}/2 - \bar{\xi}^3/6}{1-\bar{\xi}} + mL^2(V_0 - \dot{W}_1)\dot{\bar{\xi}} \times \frac{\bar{x}^2/2 - \bar{x}^3/6 - \bar{\xi}\bar{x} + \bar{\xi}^2\bar{x}/2 + \bar{\xi}^2/2 - \bar{\xi}^3/3}{(1-\bar{\xi})^2}. \tag{45}$$

Eqs. (44) and (45), with the conditions $Q = 0$ and $M = 0$ at $\bar{x} = 1$ give

$$\ddot{W}_1(1-\bar{\xi}) + (V_0 - \dot{W}_1)\dot{\bar{\xi}} = 0 \tag{46}$$

and

$$M_0 + mL^2\ddot{W}_1(1-\bar{\xi})^2/6 + mL^2(V_0 - \dot{W}_1)\dot{\bar{\xi}}(1-\bar{\xi})/3 = 0, \tag{47}$$

respectively, which can be solved to give the acceleration at the support and the dimensionless velocity of the travelling plastic hinge,

$$\ddot{W}_1 = \frac{6M_0}{mL^2(1-\bar{\xi})^2} \tag{48}$$

and

$$\dot{\bar{\xi}} = \frac{6M_0}{mL^2(\dot{W}_1 - V_0)(1-\bar{\xi})}. \tag{49}$$

The velocity $\dot{W}_1$ can be obtained from Eqs. (48) and (49) by noting that $d\dot{W}_1/dt = (d\dot{W}_1/d\bar{\xi})(d\bar{\xi}/dt)$, yielding

$$\dot{W}_1 = V_0 + \left(\dot{W}_s - V_0\right)\left(1-\bar{\xi}_0\right)\Big/\left(1-\bar{\xi}\right), \tag{50}$$

which reduces Eq. (49) to

$$\dot{\bar{\xi}} = \frac{6M_0}{mL^2(1-\bar{\xi}_0)(\dot{W}_s - V_0)} \tag{51}$$

or

$$\dot{\bar{\xi}} = -3M_0/\beta. \tag{52}$$

This equation can be integrated to yield the plastic hinge position

$$\int_{\bar{\xi}_0}^{\bar{\xi}} \mathrm{d}\bar{\xi} = \int_{t_{fa}}^{t} \frac{6M_0 \mathrm{d}t}{mL^2(1-\bar{\xi}_0)(\dot{W}_s - V_0)}, \tag{53}$$

which gives

$$\bar{\xi} = \bar{\xi}_0 + \frac{6M_0(t-t_{fa})}{mL^2(1-\bar{\xi}_0)(\dot{W}_s - V_0)} = 1 - 3M_0 t/\beta \tag{54}$$

and allows Eq. (50) to be written

$$\dot{W}_1 = V_0 - \frac{2\beta^2}{3mL^2M_0 t}. \tag{55}$$

The displacement profile of the beam can be divided into three distinct intervals, namely

$$0 \leqslant \bar{x} \leqslant \bar{\xi}, \quad w = \int_0^t V_0 \,\mathrm{d}t, \tag{56}$$

$$\bar{\xi} \leqslant \bar{x} \leqslant \bar{\xi}_0, \quad w = \int_0^t \dot{w}\,\mathrm{d}t = \int_0^{t_{fa}} \dot{w}\,\mathrm{d}t + \int_{t_{fa}}^{t^*} \dot{w}\,\mathrm{d}t + \int_{t^*}^{t} \dot{w}\,\mathrm{d}t = \int_0^{t_{fa}} V_0\,\mathrm{d}t + \int_{t_{fa}}^{t(\bar{x})} V_0\,\mathrm{d}t + \int_{\bar{x}}^{\bar{\xi}} \frac{\dot{w}}{\dot{\bar{\xi}}}\mathrm{d}\bar{\xi} \tag{57}$$

and

$$\begin{aligned} \bar{\xi}_0 \leqslant \bar{x} \leqslant 1, \quad w &= \int_0^t \dot{w}\,\mathrm{d}t \\ &= \int_0^{t_{fa}} [\dot{W}_s + (V_0 - \dot{W}_s)(1-\bar{x})/(1-\bar{\xi}_0)]\,\mathrm{d}t + \int_{t_{fa}}^{t} [\dot{W}_1 + (V_0 - \dot{W}_1)(1-\bar{x})/(1-\bar{\xi})]\mathrm{d}t, \end{aligned} \tag{58}$$

when using $\mathrm{d}t = \mathrm{d}\bar{\xi}/\dot{\bar{\xi}}$ and where $t(\bar{x}) = \beta(1-\bar{x})/3M_0$.

Integration of Eqs. (56)–(58) lead to

$$w = V_0 t \quad 0 \leqslant \bar{x} \leqslant \bar{\xi}, \tag{59}$$

$$w = \frac{\beta}{3M_0}\left\{(1-\bar{\xi})V_0 - \frac{2\beta}{mL^2}\left[\frac{\bar{\xi}-\bar{x}}{1-\bar{\xi}} + \ln\frac{1-\bar{\xi}}{1-\bar{x}}\right]\right\} \quad \bar{\xi} \leqslant \bar{x} \leqslant \bar{\xi}_0 \tag{60}$$

and

$$w = \frac{\beta}{3M_0}\left\{(1-\bar{\xi})V_0 + \frac{\beta}{mL^2}\left[\frac{2(1-\bar{x})[v(1-\bar{\xi})-1] + \bar{\xi} - 1}{1-\bar{\xi}} - 2\ln\frac{1-\bar{\xi}}{1-\bar{\xi}_0}\right]\right\} \bar{\xi}_0 \leqslant \bar{x} \leqslant 1. \tag{61}$$

At the end of this phase of motion, i.e. $\dot{\bar{\xi}} = \int \ddot{\bar{\xi}}\mathrm{d}t = 0$, from Eq. (54), or [2]

[2] This includes t_{fa} (see Eq. (53)).

$$t_{h_0} = \beta/3M_0, \tag{62}$$

the displacements at $\bar{x} = 0$ and $\bar{x} = 1$ given by Eqs. (60) and (61) are

$$W_2 = \beta V_0/3M_0 \tag{63}$$

and

$$W_1 = \frac{\beta V_0}{3M_0} - \frac{\beta^2}{3mL^2M_0}\left\{1 + 2\ln[1/(1-\bar{\xi}_0)]\right\}, \tag{64}$$

respectively.

The velocities at the support and at the mid-span at t_{h_0} are

$$\dot{W}_1 = V_0 - 2\beta/mL^2 \tag{65}$$

and

$$\dot{W}_2 = V_0, \tag{66}$$

respectively, which imply an angular kinetic energy in one-half of the beam of

$$K = \frac{2L^3}{2}\int_{1/2}^{1}(m\,\mathrm{d}\bar{x})\{\dot{\theta}(\bar{x}-1/2)\}^2 = \frac{2L^3}{2}\int_{1/2}^{1} m\left(\frac{V_0-\dot{W}_1}{L}\right)^2(\bar{x}-1/2)^2\mathrm{d}\bar{x} = \frac{mL(V_0-\dot{W}_1)^2}{24} = \frac{\beta^2}{6mL^3}, \tag{67}$$

to be absorbed by the central plastic hinge ($M_0\theta_3$) during the third phase of motion in Fig. 4(c), leading to [3]

$$\theta_3 = (mL/24M_0)(V_0-\dot{W}_1)^2 = \frac{\beta^2}{6mL^3M_0}. \tag{68}$$

The duration of the third phase of motion, t_3, is obtained from the conservation of angular momentum

$$M_0 t_3 = 2\int_0^{1/2} L^3 m\,\mathrm{d}\bar{y}\dot{\theta}\bar{y}\bar{y} = 2mL^2(V_0-\dot{W}_1)\int_0^{1/2}\bar{y}^2\,\mathrm{d}\bar{y}, \tag{69}$$

or

$$t_3 = mL^2(V_0-\dot{W}_1)/12M_0 = \beta/6M_0, \tag{70}$$

where $\bar{y} = \bar{x} - 1/2$ is an auxiliary reference system.

It is important to note that during the phase in Fig. 4(c), the beam is separated from the supports, so that a rigid body motion occurs, as well as the rotation. Thus, the beam displaces $V_r t_3$, where V_r is the rigid body velocity given by the conservation of linear momentum of the beam using Eqs. (42) and (65)

$$\int_0^1 m[V_0 - 2\beta/mL^2 + 2\beta/mL^2(1-\bar{x})]L\,\mathrm{d}\bar{x} = mLV_r, \tag{71}$$

from which follows the rigid body velocity

$$V_r = V_0 - \beta/mL^2, \tag{72}$$

which also equals

[3] Note that no unloading occurs at the central hinge because the velocity at the mid-span is greater than the residual velocity (Eq. (72)) and is greater than the velocity at the severed end. The three velocities are equal at $t = t_3$.

$$V_r = (V_0 + \dot{W}_1)/2. \tag{73}$$

The total displacements at the severed end, W_{f_1}, and at the mid-span, W_{f_2}, at the end of the third phase in Fig. 4(c) when $\dot{W}_1 = \dot{W}_2 = V_r$ are

$$W_{f_1} = W_1 + V_r t_3 - \theta_3 L/2 = \frac{\beta V_0}{2M_0} - \frac{\beta^2}{3mL^2M_0}[7/4 + 2\ln(2v/3)] \tag{74}$$

and

$$W_{f_2} = W_2 + V_r t_3 + \theta_3 L/2 = \frac{\beta}{2M_0}\left(V_0 - \frac{\beta}{6mL^2}\right), \tag{75}$$

respectively. Thus, the difference in displacement between the mid-span and the severed end is

$$W_{f_2} - W_{f_1} = \frac{\beta^2}{mL^2M_0}\left\{\frac{1}{2} + \frac{2}{3}\ln(2v/3)\right\}. \tag{76}$$

The time when rigid body motion commences is the sum of Eqs. (62) and (70),

$$t_f = \beta/2M_0 = vt_{fa}. \tag{77}$$

4.3. Rigid-body motion

Once the velocities during the third phase of motion in Fig. 4(c) become equal, at $t = t_f$ when $\dot{W}_1 = \dot{W}_2 = V_r$, then all plastic deformation ceases, and the permanently deformed beam continues to travel through space for $t > t_f$ as a rigid body, with the rigid body velocity V_r.

For the particular case when $\dot{W}_s = 0$, the rigid body velocity is

$$V_r = V_0(1 - 3/4v), \tag{78}$$

which reduces to

$$V_r = V_0/2 \quad \text{and} \quad V_r = V_0, \tag{79}$$

for $v = 3/2$ and $v \to \infty$, respectively.

It is proved in Appendix A that the above kinematically admissible solution is also statically admissible and, hence, exact.

5. Discussion

5.1. Motion before failure

The basic motivation for this study is to investigate the further plastic deformation and subsequent rigid body motion of a beam after failure. Taking, for example, the beam studied in Section 4 ($v > 3/2$), its behaviour can be described as follows.

Initially, a beam subjected to a blast loading, which is characterised by an initial velocity V_0, starts to move according to the velocity profile indicated in Fig. 4(a), i.e. a central region of the beam moves with a velocity V_0 which is faster than the section of the beam undergoing transverse shear deformations near to the supports.

For $0 < \bar{x} < \bar{\xi}_0$, the displacement is $V_0 t$, and for the portion $\bar{\xi}_0 \leqslant \bar{x} \leqslant 1$, the displacement is obtained by integrating Eq. (32),

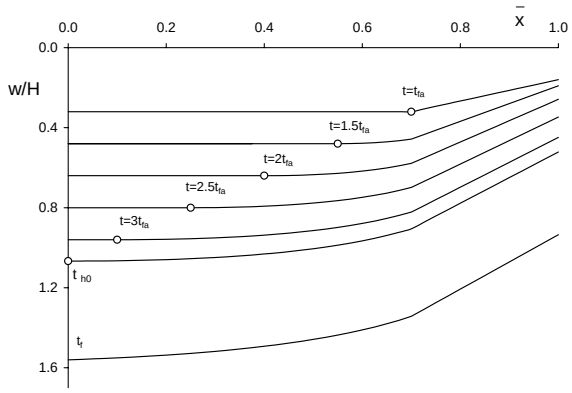

Fig. 5. Profile of a 100 mm long beam with a square cross-section of depth 10 mm, made from the aluminium alloy listed in Table 1, at various phases of motion. $v = 5$ and the initial (critical) velocity is 153.67 m/s with the circles marking the position of the plastic hinge at various times.

$$w = V_0 t - \frac{4v^2 M_0}{3mL^2} \frac{(\bar{x} - \bar{\xi}_0)}{(1 - \bar{\xi}_0)} t^2, \tag{80}$$

which is plotted in Fig. 5 for $t = t_{\mathrm{fa}}$, at the threshold of failure.

5.2. Motion after failure

Sufficiently severe impulsive velocity loadings will produce large transverse shear displacements at the supports, which causes a beam to fail at the time given by Eq. (35), when the velocity of the central part of the beam is still V_0, while at the supports it is given by Eq. (38). The plastic hinges at $\bar{\xi}_0 = \pm(1 - 3/2v)$ commence now to move inwards during the second phase of motion in Fig. 4(b) and travel with a velocity given by Eq. (52). This transient phase of motion is completed at the time given by Eq. (62), when the travelling plastic hinges coalesce at the mid-span. At the end of the second phase of motion, the beam velocities at the mid-span and at the broken ends are given by Eqs. (66) and (65), respectively. Thus, the profile of the severed beam continues to change since the transverse velocity at the centre, V_0, is different to that at the supports.

This change in profile occurs during the third phase of motion in Fig. 4(c). The central hinge continues to load at $t = t_{\mathrm{h}_0}$ and absorbs plastic energy until a time given by Eq. (77), when the beam ceases to change its shape, i.e. $\dot{W}_1 = \dot{W}_2 = V_{\mathrm{r}}$ and possesses a final rigid body velocity given by Eq. (72).

Fig. 5 illustrates the various phases of motion for a 10 mm × 10 mm square cross-section aluminium alloy beam with a flow stress $\sigma_0 = 300$ MPa, $k = 0.16$, total length of $2L = 100$ mm and subjected to an initial velocity, $V_0 = V_{0_{\mathrm{c}}} = 153.67$ m/s.

It is interesting to note that the velocities at the support and mid-span for this particular beam change according to Fig. 6. It can be seen that the initial support velocity, V_0, decreases rapidly to zero at the failure time, t_{fa}, when the impulsive velocity is the critical one i.e., $V_{0_{\mathrm{c}}}$. The severed end of the beam then resumes its motion until the final rigid body velocity is achieved at $t = t_{\mathrm{f}}$, according to Eq. (77). The figure also shows two other cases for impulsive velocities higher than the critical one.

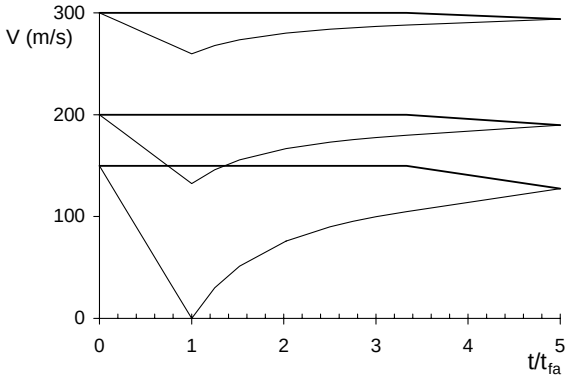

Fig. 6. Variation of transverse velocity at the support (thin line) and at the mid-span (thick line) of the aluminium alloy beam in Fig. 5 for V_0 equal 153.67, 200 and 300 m/s. Time is dimensionless with respect to the failure time corresponding to each impulsive velocity.

5.3. Residual kinetic energy

After severance, and after the stationary and travelling plastic hinges cease absorbing plastic energy, the permanently deformed beam travels through space as a rigid body, possessing a finite kinetic energy.

For beams with $v \leqslant 1$, the velocity at the support when severance occurs, which is the same as the residual velocity for the beam, is given by Eq. (5), yielding a residual, K_r, to initial, K_i, kinetic energy ratio of

$$\frac{K_r}{K_i} = 1 - \frac{2kHQ_0}{mLV_0^2}. \tag{81}$$

For the case of a beam with $1 \leqslant v \leqslant 3/2$, the rigid body velocity, Eq. (28), is associated with a kinetic energy ratio

$$\frac{K_r}{K_i} = \left(1 - \frac{v\alpha}{(4v-3)mLV_0}\right)^2, \tag{82}$$

which reduces to

$$\frac{K_r}{K_i} = 1 - \frac{4kM_0}{mLV_0^2} \tag{83}$$

and

$$\frac{K_r}{K_i} = \left(\frac{1}{2} + \sqrt{\frac{1}{4} - \frac{2kM_0}{mLV_0^2}}\right)^2 \tag{84}$$

for $v = 1$ and $v = 3/2$, respectively, and the particular case of a beam with a solid rectangular cross-section having $v = L/H$.

Further, when assuming $\dot{W}_s = 0$, this energy ratio becomes

$$\frac{K_r}{K_i} = \left(\frac{3v-3}{4v-3}\right)^2, \tag{85}$$

which is independent of the impulsive velocity. For $v = 3/2$, this ratio is 1/4, which means that a beam retains 25% of the initial kinetic energy after complete severance.

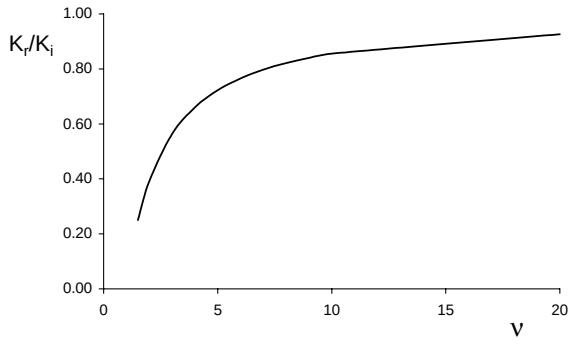

Fig. 7. Residual to initial kinetic energy ratio for different $v \geqslant 3/2$ and $\dot{W}_{\bar{s}} = 0$.

For beams with $v > 3/2$, the ratio of residual to initial kinetic energy, according to Eq. (72), is

$$\frac{K_r}{K_i} = \left(1 - \beta/mL^2V_0\right)^2, \tag{86}$$

which reduces to

$$\frac{K_r}{K_i} = \left(\frac{4v-3}{4v}\right)^2, \tag{87}$$

when $\dot{W}_{\bar{s}} = 0$, according to Eq. (38). It is evident from Fig. 7 that, for longer beams, the residual kinetic energy can be significant. For instance, for the beam examined in Fig. 5, $v = 5$, and the residual kinetic energy is $K_r = 0.723K_i$. It is clear that the kinetic energy in a beam after severance could inflict damage on any object caught in the beam trajectory.

5.4. Energy partitioning

The energy dissipated during the various phases of motion in the beam analyses may be partitioned into bending and shear energies. Considering the case $v \geqslant 3/2$, the shear energy at the supports during the first phase of motion, i.e. for $0 \leqslant t \leqslant t_{fa}$ and for one-half of the beam, is given by

$$K_{s_s} = \frac{2vM_0}{L}\left(V_0 t - \frac{4v^2M_0t^2}{3mL^2}\right). \tag{88}$$

The bending energy has three components. One is due to bending at the stationary plastic hinge during the first phase of motion before severance,

$$K_{b_s} = M_0(V_0t - W_s)/(L - \xi_0) = 8v^3M_0^2t^2/9mL^3, \tag{89}$$

which is valid for $0 \leqslant t \leqslant t_{fa}$.

Another component is the bending energy absorbed during the propagation of the bending hinge after severance during the second phase of motion, valid for $t_{fa} \leqslant t \leqslant t_{h_0}$,

$$K_{b_m} = -(M_0/L)\int_{t_{fa}}^{t}\left[\partial\dot{w}/\partial\bar{x}\right]\mathrm{d}t = \frac{2\beta^2(-\beta + 2vM_0t)}{9mL^3M_0t}. \tag{90}$$

The angular kinetic energy in Eq. (67) during the third phase of motion causes additional displacements at the severed end and at the mid-span, as observed by Eqs. (74) and (75), respectively. Eq. (67) gives the plastic bending energy consumed in the third phase of motion and can be written as

$$\frac{K_{b_r}}{K_i} = \frac{3}{16v^2}\left\{1 - \sqrt{1 - (V_{0_c}/V_0)^2}\right\}^2, \tag{91}$$

when using Eq. (41) and making it dimensionless with respect to the input energy. Eq. (91) shows, for a given value of v, that the dissipation of the initial kinetic energy by bending, once the transient phase after severance ceases, is largest when the impulsive velocity equals the critical value V_{0_c}.

The transient phase in Fig. 4(b), when the plastic hinge propagates from $\bar{x} = \bar{\xi}_0$ to $\bar{x} = 0$, and the final bending phase in Fig. 4(c), both of which develop after beam severance, are unique features of the present impact problem. It is then interesting to evaluate some ratios relating the various energies in these phases of motion. For instance, the ratio between the bending energy dissipated during the hinge propagation phase in Fig. 4(b) and the bending energy absorbed by the stationary plastic hinge at the mid-span in Fig. 4(c), is given by

$$K_{b_r}/K_{b_m} = 3/4(2v - 3). \tag{92}$$

A plot of this equation is shown in Fig. 8, where it is evident that, for $v \geqslant 1.875$, the bending energy absorbed during the hinge propagation phase after severance is greater than the bending energy absorbed by the stationary hinge at the mid-span during the final post-severance phase.

The plastic energy absorbed after severance during the third and second phases is given by the ratios

$$r_1 = \frac{K_{b_r}}{K_{s_s} + K_{b_s}} = \frac{3}{8v}\frac{1 - \sqrt{1 - (V_{0_c}/V_0)^2}}{2 + \sqrt{1 - (V_{0_c}/V_0^2)}} \tag{93}$$

and

$$r_2 = \frac{K_{b_m}}{K_{s_s} + K_{b_s}} = \frac{v - 3/2}{v}\frac{1 - \sqrt{1 - (V_{0_c}/V_0)^2}}{2 + \sqrt{1 - (V_{0_c}/V_0)^2}}, \tag{94}$$

respectively, when made dimensionless with respect to the total energy absorbed before severance during the first phase of motion.

For the particular case when $V_0 = V_{0_c}$, these ratios become

$$r_1 = \frac{3}{16v} \tag{95}$$

and

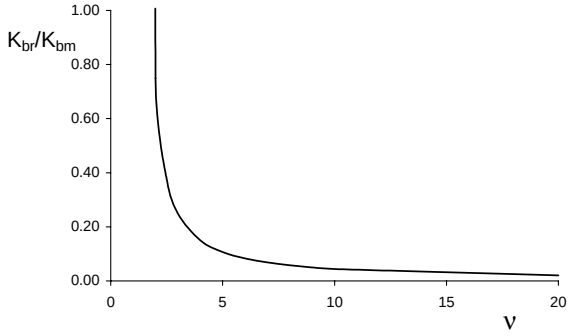

Fig. 8. Ratio between the bending energies after severance for $v \geqslant 3/2$.

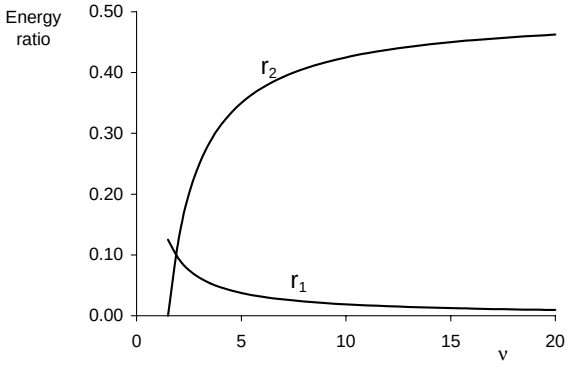

Fig. 9. Energy ratios for $V_0 = V_{0_c}$.

$$r_2 = \frac{2v - 3}{4v}, \tag{96}$$

which are plotted in Fig. 9.

Fig. 10 shows the evolution with time of the shear and bending energies during the various phases of motion for the beam illustrated in Fig. 5.

5.5. Critical velocity

The dimensionless critical velocities for the beams are shown in Fig. 11 when using

$$\bar{V}_{0_c} = 2\sqrt{v}, \quad v \leqslant 1, \tag{97}$$

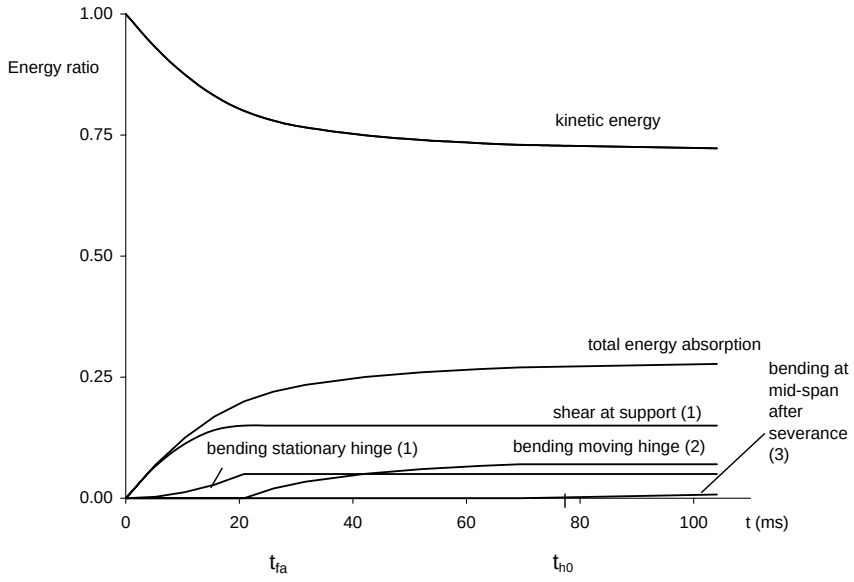

Fig. 10. Time evolution of the dimensionless energy partition for the beam illustrated in Fig. 5. The total duration of motion is 104.1 μs. Phases of motion are indicated in parentheses.

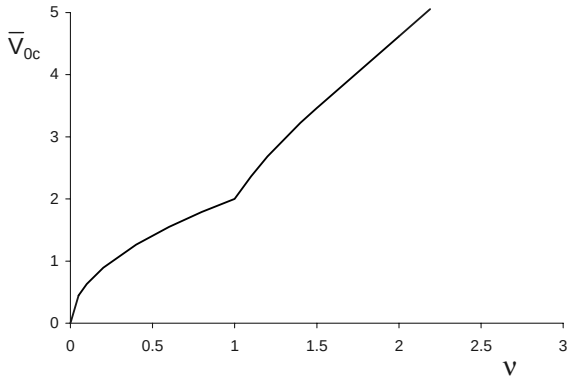

Fig. 11. Dimensionless critical velocity as a function of v.

$$\bar{V}_{0_c} = 2\sqrt{4v-3}, \quad 1 < v \leqslant 3/2 \tag{98}$$

and

$$\bar{V}_{0_c} = 4v/\sqrt{3}, \quad v > 3/2, \tag{99}$$

where $\bar{V}_{0_c} = V_{0_c}/(kHM_0/mL^2)^{1/2}$.

5.6. Failure criterion

It is interesting to enquire whether or not the elementary transverse shear failure criterion given by Eq. (2) has any theoretical support. Here, we explore a simple ductile damage mechanics model suggested by Lemaitre (1985a,b).

The beam motion has been analysed using a rigid, perfectly plastic material model. This implies that any elastic effects are of second order importance in the beam response. In this section, however, we use an elastic, perfectly plastic material in order to allow for the necessary elastic modulus degradation used in a failure criterion taken from the Damage Mechanics framework. Also, the so called crack closure effect is here disregarded since failure at the supports occurs with no change in the direction of motion of a beam.

The damage evolution is obtained by integrating the equation

$$\dot{D} = \tilde{\sigma}_{\mathrm{eq}}^2 R_{\bar{\nu}} \dot{p} \bar{H}(p - p_{\mathrm{D}})/2E\bar{S}, \tag{100}$$

where D is the damage, E is the elastic modulus and $\bar{S}$ is a material constant. $\bar{H}$ is the Heaviside function which is equal 1 or zero if the accumulated plastic strain, p, is greater or smaller than the threshold accumulated plastic strain, p_{D}, respectively. The term $R_{\bar{\nu}}$ is given by

$$R_{\bar{\nu}} = 2(1+\bar{\nu})/3 + 3(1-2\bar{\nu})(\sigma_{\mathrm{h}}/\sigma_{\mathrm{eq}})^2 \tag{101}$$

and takes into account the Poisson's ratio, $\bar{\nu}$, and the triaxiality, a hydrostatic to equivalent stress ratio, $\sigma_{\mathrm{h}}/\sigma_{\mathrm{eq}}$. Also, the effective stress, $\tilde{\sigma}_{\mathrm{eq}}$, is defined by $\tilde{\sigma}_{\mathrm{eq}} = \sigma_{\mathrm{eq}}/(1-D)$, whereas the accumulated plastic strain rate is defined by $\dot{p} = \sqrt{(2/3)\dot{\varepsilon}_{ij}^{\mathrm{p}}\dot{\varepsilon}_{ij}^{\mathrm{p}}}$, which becomes an equivalent strain, $\varepsilon_{\mathrm{eq}}$, when integrating for the case of a proportional loading regime.

For a rigid, perfectly plastic material with an effective flow stress, σ_0, Eq. (100) can be integrated to give

$$D = \sigma_0^2 R_{\bar{\nu}}(\varepsilon_{\mathrm{eq}} - \varepsilon_{\mathrm{D}})/2E\bar{S} \quad \text{for } \varepsilon_{\mathrm{eq}} \geqslant \varepsilon_{\mathrm{D}}. \tag{102}$$

Table 1
Damage mechanics material parameters for a mild steel (Alves and Jones, 2002b) and for aluminium (Lemaitre, 1992)

Material	σ_0 (MPa)	E (GPa)	ρ (kg/m^3)	$\bar{S}$ (MPa)	$\bar{v}$	ε_D	D_{cr}
Steel	480	209.8	7800	0.6	0.287	0.17	0.45
Aluminium	300	72	2710	1.7	0.32	0.03	0.23

If it is assumed that the transverse shear strain at the supports is (Alves and Jones, 2002a)

$$\gamma = W_s/(l_Q/2), \tag{103}$$

where $l_Q = (3-\sqrt{6})H/2$ is the length of a shear hinge in a simply supported beam based on the transverse shear force acting in a beam with $v \geqslant 3/2$, then the equivalent strain becomes

$$\varepsilon_{eq} = \gamma/\sqrt{3} = [(4/3)/(\sqrt{3}-\sqrt{2})][W_s/H]. \tag{104}$$

Eq. (102) can now be written as

$$W_{s_{cr}} = (3/2)(\sqrt{3}-\sqrt{2})(E\bar{S}D_{cr}/R_{\bar{v}}\sigma_0^2 + \varepsilon_D/2)H, \tag{105}$$

at incipient failure, i.e. $D = D_{cr}$.

A comparison of Eqs. (2) and (105) gives at once that

$$k = (3/4)(\sqrt{3}-\sqrt{2})(2E\bar{S}D_{cr}/R_{\bar{v}}\sigma_0^2 + \varepsilon_D). \tag{106}$$

Eq. (106) for the specific mild steel material described in Alves and Jones (2002b) and listed in Table 1 predicts

$$k = 0.18, \tag{107}$$

when assuming

$$R_{\bar{v}} = (2/3)(1+\bar{v}), \tag{108}$$

which corresponds to a state of pure shear, $\sigma_h = 0$.

Similarly, for an aluminium alloy beam, the value of k according to Eq. (106) is also 0.18 when using the data listed in Table 1. The equivalent strain in the above calculations corresponds to a pure shear state, since the bending moment is zero at the simple support.

It is interesting to note that an increase of strain rate would increase the material flow stress, which decreases quadratically the value of k when the other parameters remain unchanged. Hence, the greater the impulsive load, the smaller the displacement to failure.

More general expressions are presented in Alves and Jones (2002a) which may be used for the prediction of failure in beams having more complex stress states than the pure shear case examined here.

6. Conclusions

A theoretical analysis is presented for the severance and subsequent behaviour of a simply supported rigid, perfectly plastic beam subjected to a blast loading which may be characterised as an impulsive velocity distributed uniformly throughout the span. The results indicate that, after severance, the remaining kinetic energy in the beam causes it to change shape due to stationary and travelling plastic hinges which continue to absorb energy. This change of shape after failure has relevance for forensic investigations.

Moreover, after the plastic energy absorption ceases, a residual kinetic energy remains in a beam, which depends on the beam length to thickness ratio, and can be a significant proportion of the initial kinetic

energy. Hence, the detached beam has a rigid body motion which can be potentially harmful to any items lying within the trajectory.

It is shown that a simple failure criterion, in which severance occurs when the shear displacement reaches a certain fraction of the beam thickness, can be derived from a more rigorous approach based on Continuum Damage Mechanics.

It appears that similar theoretical solutions can also be obtained for fully clamped beams and simply supported circular plates. The solution here presented could eventually be developed further for a wider range of structures with various boundary conditions and dynamic loadings, although in some cases, simple numerical schemes might be required. Exact theoretical solutions, as those presented here, can be used to check the accuracy of finite element solutions, which can then be used for more complex problems associated with the post-failure motion of structures subjected to large dynamic loads.

Appendix A. Static admissibility of the solutions

It is important to verify whether or not the above theoretical solutions violate the yield criterion, at any point of the beam span and at any time. This is achieved by investigating the transverse shear force, Q, and the bending moment, M, and seeking the conditions when they would pierce a square shaped yield surface relating Q and M.

If it can be proven that the above bending moment and shear force distributions do not violate the yield criterion, then the solution is called statically admissible. Moreover, since the theoretical solution is also kinematic admissible, then it is exact in the context of a rigid, perfectly plastic theory.

The theoretical solution has been shown to be exact by Jones (1989) up to the point of severance. Thus, it is necessary only to examine the subsequent response.

A.1. $v < 1$

For beams with $v < 1$, the moment distribution before severance is readily obtained as $M/M_0 = v(1 - \bar{x}^2)$, with both the first and second derivatives negative along the beam span. The transverse shear force is $Q/Q_0 = -\bar{x}$, giving $Q/Q_0 \leqslant 1$ for any value of $\bar{x}$. Hence, no yield violation occurs during this phase of motion.

After severance, the shear force and bending moment are zero at the supports and along all the beam span according to the equilibrium equations when the beam has a straight profile. Therefore, it travels as a rigid body and no yield violation occurs with the solution being exact.

A.2. $1 \leqslant v < 3/2$

For beams with $1 \leqslant v \leqslant 3/2$, Section 3, Eqs. (19), (21) and (22) give the transverse shear force after severance

$$Q = -6M_0\bar{x}(1 - \bar{x})/L, \tag{A.1}$$

with $Q = 0$ at $\bar{x} = 0$ and at $\bar{x} = 1$, as required from the symmetry and boundary conditions after severance. The spatial derivative of Eq. (A.1) is zero at $\bar{x} = 1/2$, giving a minimum value of the transverse shear force

$$Q_{\min}/Q_0 = -3/4v. \tag{A.2}$$

Hence, the minimum transverse shear force ratio lies between $-1/2$ and $-3/4$.

It is also necessary to explore the bending moment behaviour along the beam span and throughout the beam response. The bending moment for beams with $1 \leqslant v \leqslant 3/2$ is given by Eqs. (20)–(22), or

$$M/M_0 = 1 - 3\bar{x}^2 + 2\bar{x}^3, \tag{A.3}$$

with $M/M_0 = 1$ and zero at $\bar{x} = 0$ and at $\bar{x} = 1$, respectively.

Since the spatial derivative of the bending moment at $\bar{x} = 0$ and at $\bar{x} = 1$ is zero, it is only necessary to prove that the second derivative is positive at $\bar{x} = 1$ and negative at $\bar{x} = 0$. The expression

$$\mathrm{d}^2M/\mathrm{d}x^2 = (6M_0/L^2)(-1 + 2\bar{x}), \tag{A.4}$$

is negative for $0 \leqslant \bar{x} \leqslant 1/2$ and positive for $1/2 \leqslant \bar{x} \leqslant 1$, so that the solution is statically admissible and is valid for $1 \leqslant v \leqslant 3/2$.

A.3. $v \geqslant 3/2$

For beams with $v \geqslant 3/2$, Section 4, the solution for the first phase of motion in Fig. 4(a) is proven to be statically admissible in Jones (1989).

In the second phase of motion in Fig. 4(b), where the hinges propagate towards the beam centre, the transverse shear force is

$$Q = \partial M/\partial x = (6M_0/L)(\bar{x} - 1)(\bar{x} - \bar{\xi})/(1 - \bar{\xi})^3, \tag{A.5}$$

which is zero at $\bar{x} = 1$ and at $\bar{x} = \bar{\xi}$.

The derivative of Eq. (A.5)

$$\partial Q/\partial \bar{x} = (6M_0/L)(2\bar{x} - \bar{\xi} - 1)/(1 - \bar{\xi})^3, \tag{A.6}$$

is positive at $\bar{x} = 1$ and negative at $\bar{x} = \bar{\xi}$. Also, $\partial Q/\partial \bar{x} = 0$ gives $\bar{x} = (1 + \bar{\xi})/2$, which is the position where the transverse shear force attains a minimum value of

$$Q_{\min} = -3M_0/2L(1 - \bar{\xi}) \geqslant -Q_0/2. \tag{A.7}$$

The bending moment distribution in Eq. (45) can be reduced to

$$M/M_0 = \frac{(\bar{x} - 1)^2(2\bar{x} + 1 - 3\bar{\xi})}{(1 - \bar{\xi})^3}, \tag{A.8}$$

whose first derivative, Eq. (A.5), is zero at $\bar{x} = \bar{\xi}$ and $\bar{x} = 1$.

The second derivative of Eq. (A.8) is negative at $\bar{x} = \bar{\xi}$, positive at $\bar{x} = 1$ and is zero at $\bar{x} = (1 + \bar{\xi})/2$, where $M/M_0 = 1/2$.

In the final phase of motion, Fig. 4(c), when the rigid body rotation, θ_3, occurs, the bending moment distribution and the transverse shear force are given by

$$M/M_0 = 1 + \bar{x}^2(2\bar{x} - 3) \quad \text{and} \quad Q/Q_0 = -3\bar{x}(1 - \bar{x})/v. \tag{A.9}$$

A minimum value for the transverse shear force occurs at $\bar{x} = 1/2$ and its second derivative is always positive so no yield violation occurs. The first derivative of the bending moment is zero at $\bar{x} = 0$ and $\bar{x} = 1$, while the second derivative is negative in the interval $0 \leqslant \bar{x} < 1/2$ and positive in the interval $1/2 < \bar{x} \leqslant 1$, with zero at $\bar{x} = 1/2$. Hence, no yield violation occurs in any phase of motion and the solution is statically admissible.

References

Alves, M., Jones, N., 2002a. Impact failure of beams using damage mechanics: Part I—analytical model. International Journal of Impact Engineering 27 (8), 837–861.

Alves, M., Jones, N., 2002b. Impact failure of beams using damage mechanics: Part II—application. International Journal of Impact Engineering 27 (8), 863–890.

Bammann, D., Chiesa, M., Horstemeyer, M., Weingarten, L., 1993. Failure in ductile materials using finite element methods. In: Jones, N., Wierzbicki, T. (Eds.), Structural Crashworthiness and Failure. Elsevier Science Publishers, Barking, Essex, pp. 1–54.

Holmes, B., Kirkpatrick, S., Simons, J., Giovanola, J., Seaman, L., 1993. Modeling the process of failure in structures. In: Jones, N., Wierzbicki, T. (Eds.), Structural Crashworthiness and Failure. Elsevier Science Publishers, Ltd., Barking, Essex, pp. 55–93.

Johnson, W., 1990. The elements of crashworthiness: scope and actuality. Proceedings of the Institution of Mechanical Engineers 204, 255–273.

Jones, N., 1976. Plastic failure of ductile beams loaded dynamically. Transactions of ASME, Journal of Engineering for Industry 98 (1), 131–136.

Jones, N., 1989. Structural Impact. Cambridge University Press, Cambridge.

Jones, N., Oliveira, J., 1979. The influence of rotatory inertia and transverse shear on the dynamic plastic behaviour of beams. Transactions of ASME, Journal of Applied Mechanics 46 (2), 303–310.

Jones, N., Wierzbicki, T., 1987. Dynamic plastic failure of a free–free beam. International Journal of Impact Engineering 6 (3), 225–240.

Jouri, W., Jones, N., 1988. The impact behaviour of aluminium alloy and mild steel double-shear specimens. International Journal of Mechanical Sciences 30 (3/4), 153–172.

Lemaitre, J., 1985a. A continuous damage mechanics model for ductile fracture. Journal of Materials and Technology 107, 83–89.

Lemaitre, J., 1985b. Coupled elasto-plasticity and damage constitutive equations. Computer Methods in Applied Mechanics and Engineering 51, 31–49.

Lemaitre, J., 1992. A Course on Damage Mechanics. Springer-Verlag, Berlin.

Yang, J.L., Xi, F., 2003. Experimental and theoretical study of free–free beam subjected to impact at any cross-section along its span. International Journal of Impact Engineering 28 (7), 761–781.

Yang, J.L., Yu, T.X., Reid, S.R., 1998. Dynamic behaviour of a rigid perfectly plastic free–free beam subjected to step-loading at any cross-section along its span. International Journal of Impact Engineering 21 (3), 165–175.

Yu, T.X., Yang, J.L., Reid, S.R., Austin, C.D., 1996. Dynamic behaviour of elastic–plastic free–free beams subjected to impulsive loading. International Journal of Solids and Structures 33 (18), 2659–2680.

Yu, T.X., Yang, J.L., Reid, S.R., 2001. Deformable body impact: dynamic plastic behaviour of a moving free–free beam striking the tip of a cantilever beam. International Journal of Solids and Structures 38, 261–287.